Sergey V Sukhomlinov[1] **and Martin H Müser**[1,2]

E-mail: martin.mueser@mx.uni-saarland.de
[1] John von Neumann Institute for Computing and Jülich Supercomputing Centre, FZ Jülich, 52425 Jülich, Germany
[2] Dept. of Materials Science and Engineering, Saarland University, 66123 Saarbrücken, Germany

Constraints on phase stability, defect energies, and elastic constants of metals described by EAM-type potentials

Abstract. We demonstrate that the embedded-atom method and related potentials predict many dimensionless properties of simple metals to depend predominantly on a single coefficient μ, which typically lies between 0.3 and 0.45. Among other relations presented in this work, we find that $E_c \propto Z^\mu$, $E_v/E_c = \mu$, and $G/B \propto \mu$ hold within 25% accuracy and also find a linear dependence of the melting temperature on μ. The used variables are cohesive energy E_c, coordination number Z, vacancy energy E_v, and bulk modulus B, while G is the average of ordinary and tetragonal shear modulus. We provide analytical arguments for these findings, which are obeyed reasonably well by several metals.

PACS numbers: 34.20.Cf, 62.20.D, 61.72.Bb, 65.40.gp

1. Introduction

Large-scale simulations of metals [1, 2, 3, 4, 5] are frequently based on atomistic potentials deriving their theoretical justification from quasi-atom theory (QAT) [6]. It states that the energy gained when placing an atom into a configuration of other atoms depends in leading order on the electronic density that exists at the embedding site before the extra atom is added. While the embedded-atom method (EAM) [7, 8, 9] is arguably the most popular QAT-based potential, different formulations exist that — like EAM — contain the following three ingredients: a two-body pair repulsion between cores, $U_{\mathrm{R}}(r_{ij})$, the electronic charge density of individual atoms $\phi(|\mathbf{r}-\mathbf{r}_j|)$ adding up to the charge density $\rho_i = \sum_{j\neq i}\phi(r_{ij})$ at the embedding site $\mathbf{r}_i$, and the embedding function $F(\rho_i)$. The total energy in QAT-inspired potentials thus reads

$$U_{\mathrm{T}} = \sum_{i,j>i} U_{\mathrm{R}}(r_{ij}) + \sum_i F(\rho_i) \tag{1}$$

in its most generic form, which does not include square-gradient [6, 10] or related corrections [11] derived from higher-order derivatives of the charge density at the embedding site. Approaches merely differ in their functional forms assumed for repulsion, charge density, and embedding function.

The list of QAT-based potentials include the Gupta potential [12], which originally was proposed as the second-order moment expansion of a tight-binding model [12, 13, 14], the glue potential [15], and the Finnis-Sinclair potential [16], to name a few. Although EAM is by far the most used QAT potential, it requires complex input in form of numerical tables and when tested for transferability, e.g., towards structures with small coordination, EAM apparently falls behind much simpler QAT variants [11, 17]. In particular the four-parameter Gupta potential clearly outperforms EAM (original and reparametrized) as well as other QAT variants when fitted to either copper [11] or aluminum [17] structures encompassing clusters, one-dimensional chains, two-dimensional tilings, and three-dimensional crystals. Adding complexity to the simple functional dependencies of the Gupta potential (exponential two-body repulsion, exponential charge density of atoms, and a square-root for the embedding energy) improves fits to a broad set of structures at most marginally but in most cases deteriorates transferability [11, 17]. We therefore see the Gupta potential as the most suitable QAT variant to investigate the intrinsic properties and limitations of the class of potentials whose total energy is given by equation (1). Results obtained for the analytically amenable Gupta potential should therefore also relate to other EAM-type potential of similar accuracy and transferability.

Despite their wide-spread use, only few *systematic* studies [11, 17, 18] of the *generic* properties of EAM-type potentials seem to exist. Most works are instead limited to the question of how well a fixed functional form of a potential can minimize an arbitrarily chosen χ^2 penalty function on a small set of properties and metals. However, it has not yet been addressed how different properties, as predicted by QAT-based potentials, correlate (irrespective of a given parameterization) and to what degree real metals show this correlation. For example, it is not clear why some defect energies cannot be well described or if it is possible to fine tune a vacancy energy (expressed in units of the cohesive energy) independently of the shear modulus (expressed in units of the bulk modulus). Although these issues have been touched upon to some degree, e.g., it is well known that EAM-type potentials usually give unsatisfactory surface energies [19, 20, 21], or, that hcp structures have only three

rather than five fully independent elastic constants [22, 23], there are no closed-form analytical expressions giving general answers to the just-raised questions. Moreover, it appears to have remained unnoticed hitherto that a single (relevant) dimensionless parameter determines many dimensionless properties in the Gupta potential. This restriction may lie at the root of why different materials properties cannot be fine tuned simultaneously in the realm of the considered class of potentials.

In this work, we investigate numerically but also analytically the generic properties of the Gupta potential. For comparison, we also study an alternative potential similar to the one proposed by Sutton and Chen [24]. The goal is to better understand the intrinsic limitations of this class of potentials and to identify simple rules that allow one to assess the degree of accuracy in which a given element can possibly be described without introducing fundamental modifications to the formalism. The remainder of this article is organized as follows: In section 2 we introduce the two investigated potentials. Section 3 examines if these two potentials can identify bcc as energetically more favorable than fcc. Defect energies and elastic properties are then investigated in sections 4 and 5, respectively. Section 6 contains an analysis of how different (dimensionless) properties correlate, such as shear modulus in units of the bulk modulus and $k_B T_\mathrm{m}$ divided by the cohesive energy, where T_m is the melting temperature. Conclusions are drawn in section 7.

2. Investigated potentials

The total potential energy of a (mono-atomic) system described by the Gupta potential can be written as

$$U_\mathrm{T} = \sum_{i,j>i} V_\mathrm{R} \exp(-r_{ij}/\sigma_\mathrm{R}) - W \sum_i \sqrt{\rho_i} \tag{2}$$

with

$$\rho_i = \sum_{j \neq i} \exp(-r_{ij}/\sigma_\mathrm{Q}). \tag{3}$$

Here, the parameters V_R and W have unit of energy while σ_R and σ_Q have unit of length. We note that element-specific prefactors for the estimated charge-density, ρ_i, have to be used when considering alloys. When written in this form, the potential for a mono-atomic system contains two dimensionless variables, that is, V_R/W and $\sigma_\mathrm{R}/\sigma_\mathrm{Q}$. Numerical values for the Gupta potential parameters can be taken from a study by Karolewski [25], who parameterized the Gupta potential in the context of second-moment tight-binding potentials for a total of 32 metals.

The various terms of the Gupta potential were motivated in the original paper [12] within the tight-binding approximation as well as in a later study by Cleri and Rosato, [14] who criticized the interpretation of the approach within the conventional EAM picture. However, it appears as though the employed embedding functions can also be obtained directly within effective-medium theory [26], which is analogous to QAT, by embedding atoms into a constant electron-density background.

In some cases, we focus our analysis on copper, in which case we use the parameters presented in previous, own work [11], i.e., $W = 8.227$ eV, $\sigma_\mathrm{Q} = 0.6404$ Å, and the dimensionless parameters $V_\mathrm{R}/W = 1183$ and $\sigma_\mathrm{R}/\sigma_\mathrm{Q} = 0.3567$, which yields a bond length of $a_0 = 4.03\ \sigma_\mathrm{Q}$ in the fcc phase. Karolweski's parameters for copper read $W = 12.568$ eV, $\sigma_\mathrm{Q} = 0.6404$ Å, and $V_\mathrm{R}/W = 896$ and $\sigma_\mathrm{R}/\sigma_\mathrm{Q} = 0.4149$. The small differences between our [11] and Karolewski's [25] parameters supposedly arise from

the fitting procedures. Karolewski determined the adjustable parameters by fitting to elastic and defect properties of fcc copper, while we optimized the parameters on a set of defect-free copper structures ranging from the dimer via the linear chain and various tilings to bulk structures.

In most cases, we use $\sigma_{\mathrm{R}}/\sigma_{\mathrm{Q}}$ as a (quasi-continuous) variable. One then needs to fix the ratio V_{R}/W, or, alternatively the ratio a_0/σ_{Q}, where a_0 represents the bond length of the given metal in the fcc structure. As a default value, we choose $a_0/\sigma_{\mathrm{Q}} = 4$, for mainly two reasons. First, it fits our parameterization of copper reasonably well. Second and more importantly, it is at the lower end of values proposed by Karolewski, thereby being representative of those cases, in which the nearest-shell approximation may be the least justified.

Various classes of EAM-type potentials exist in addition to those isomorphic to Gupta, in particular that introduced by Finnis and Sinclair [16]. Sutton and Chen proposed a simple and also successful form of the Finnis-Sinclair-type potential [24], which we consider here for comparison in a slightly altered form. We combine the used expression for the electron charge density, which is a $1/r^6$ power law, and replace the original repulsion, also a power law, with a supposedly more realistic exponential repulsion. Thus, the potential energy can be cast as

$$U_{\mathrm{T}} = V_{\mathrm{R}} \left\{ \sum_{i,j>i} \exp(-r_{ij}/\sigma_{\mathrm{R}}) - \sum_i \sqrt{\sum_{j\neq i} (\sigma_{\mathrm{Q}}/r_{ij})^6} \right\} \tag{4}$$

so that it only depends on one dimensionless variable $\sigma_{\mathrm{Q}}/\sigma_{\mathrm{R}}$. This time and in contrast to the Gupta potential, one cannot relate this ratio to a meaningful dimensionless range of adhesion (expressed in units of σ_{R}), since the assumed $1/r^6$ decay of the electronic density is scale free. We note in passing that, in principle, the singularity of the embedding density needs to be obliterated when two atoms approach each other closely to avoid a collapse into unphysical structures. This can be achieved, for example, by making σ_{Q} distance dependent at small r_{ij}. However, such a precautionary measure is not needed when only small deformations of structures around either fcc or bcc are considered, as long as $\sigma_{\mathrm{Q}}/\sigma_{\mathrm{R}}$ is small enough for the dimer to develop a local energy minimum at a finite bond length.

3. Crystal phase stability

In leading order, the energetics of crystalline structures can be estimated by only considering interactions of atoms with their nearest neighbors. This can be seen, for example, from the numerical values obtained for σ_{Q} in the Gupta potential [25], which are always much smaller than the nearest-neighbor spacing a_0. Thus, for most phases, the contribution of the embedding density from non-nearest neighbors is typically at most in the order of 20%. The one possible exception for simple lattices is bcc, where next-nearest neighbors are only $2/\sqrt{3}$ times more distant than the nearest ones. Since bcc structures play an important role in this work, we therefore often include next-nearest neighbors into our analysis. This moves the leading error to the embedding density to less than 10% for physically meaningful parameterizations.

Although the contribution of distant shells to the cohesive energy E_{c} is small, so is the difference between the (predicted) cohesive energies of bcc and fcc. It is therefore possible to construct (analytical) EAM potentials [27, 28] which give bcc as more stable than fcc, given that the charge density cutoff lies between the the

second and third neighbors in bcc but between the first and second neighbors in fcc. To evaluate energy differences between phases accurately, one should therefore either include sufficiently many neighbor shells or consistently estimate the cutoff correction, e.g., in a mean-field or mean-density approximation. In this section, we explore both analytically and numerically how the way in which charge density and short-range potential are cut off affects the cohesive energy differences between ideal fcc and bcc. Since the energy differences between fcc and hcp are marginal, as long as no the potential has no explicit or implicit angle dependence, we do not consider hcp in this study.

3.1. Gupta potential

For sufficiently small values of σ_Q/a_0, one can ignore the effect of the next-nearest neighbor shell. The bond length, a_0, and the binding energy per atom, E_c, then are [11]

$$a_0 = \frac{2\sigma_\mathrm{Q}\sigma_\mathrm{R}}{2\sigma_\mathrm{Q}-\sigma_\mathrm{R}} \ln\left(\sqrt{Z}\frac{\sigma_\mathrm{Q}V_\mathrm{R}}{\sigma_\mathrm{R}W}\right) \tag{5}$$

$$E_\mathrm{c} = Z_0^\mu E_\mathrm{d}, \tag{6}$$

with

$$\mu = \frac{\sigma_\mathrm{Q}-\sigma_\mathrm{R}}{2\sigma_\mathrm{Q}-\sigma_\mathrm{R}} \tag{7}$$

$$E_\mathrm{d} = \frac{2\sigma_\mathrm{Q}-\sigma_\mathrm{R}}{2\sigma_\mathrm{R}}\left(\frac{W}{V_\mathrm{R}}\frac{\sigma_\mathrm{R}}{\sigma_\mathrm{Q}}\right)^{2\sigma_\mathrm{Q}/(2\sigma_\mathrm{Q}-\sigma_\mathrm{R})} V_\mathrm{R}, \tag{8}$$

assuming simple crystalline structures, where all atomic positions are equivalent. Thus, the cohesive energy of a Gupta crystal is only Z_0^μ times the binding energy of a dimer, E_d, rather than $Z_0 E_\mathrm{d}$, which would be a reasonable approximation for a short-ranged two-body potential. This is quite a significant difference because typical values for μ range from roughly 0.2 to 0.45. Assuming that the potential is sufficiently accurate for a given metal, the value of μ can be obtained from the dependence of the cohesive energy on the coordination number, though one may want to exclude dimers from the determination of μ, because square-gradient corrections may be particularly large, or, if experimental data were used, the dimer ground state could be in a triplet state.

From equation (6) follows that large coordination, i.e., $Z_0 = 12$, is preferred if $\sigma_\mathrm{Q} > \sigma_\mathrm{R}$ while dimerization occurs for $\sigma_\mathrm{Q} < \sigma_\mathrm{R} < 2\sigma_\mathrm{Q}$. For typical parameterizations one would find that in the nearest-neighbor approximation the fcc binding energy exceeds that of bcc by 12% to 20%. We next explore if including next-nearest or more distant neighbor interactions can change this ranking and turn the bcc crystal energetically favorable over fcc. Such a scenario could appear possible in light of the argument that bcc effectively corresponds to $Z_0 = 14$, as the second shell with six atoms is very close to the first one having eight.

The potential energy per particle of an unstrained crystal with arbitrary cutoff radius can be written as

$$u = \frac{\tilde{V}_\mathrm{R}}{2}\sum_s Z_s\tilde{v}_s - \tilde{W}\sqrt{\sum_s Z_s\tilde{w}_s} \tag{9}$$

where Z_0, Z_1, $\cdots$ are the number of atoms in the nearest, next-nearest-neighbor, etc. shell, respectively, and

$$\tilde{V}_\mathrm{R} = V_\mathrm{R} \exp\{-a_0/\sigma_\mathrm{R}\} \tag{10}$$

$$\tilde{W} = W \exp\{-a_0/2\sigma_\mathrm{Q}\} \tag{11}$$

$$\tilde{v}_s = \exp\{-(d_s-1)a_0/\sigma_\mathrm{R}\} \tag{12}$$

$$\tilde{w}_s = \exp\{-(d_s-1)a_0/\sigma_\mathrm{Q}\}. \tag{13}$$

Here, we have introduced $d_s = a_s/a_0$ as the ratio of spacing of an atom in the s'th shell and the nearest-neighbor ($s = 0$) shell. This representation of the energies proves particularly useful in the evaluation of elastic constants.

Unfortunately, there are no closed-form analytical expression for either the bond length or cohesive energy beyond the nearest-shell approximation when taking V_R, W, σ_R, and σ_Q as given. However, numerical estimates are readily obtained for arbitrary choices of (Z_0, Z_1, d_1), including those representative for fcc (12, 6, $\sqrt{2}$) and bcc (8, 6, $2/\sqrt{3}$). As revealed in figure 1, the ratio $E_\mathrm{c}(\mathrm{fcc})/E_\mathrm{c}(\mathrm{bcc})$ drops significantly from the first estimate of 12%-20% to 5%-7% but still remains above one if a direct summation is truncated after next-nearest neighbors. When including more distant neighbors and continuum corrections to the direct summation, a small domain appears (outside the shown parameter range), where bcc can be made marginally more stable than fcc – but never more than 0.4%. It is therefore not possible to make the Gupta potential clearly prefer bcc over fcc at zero stress and temperature. While there is a small domain in which the cohesive energy of bcc is marginally larger than that of fcc — it just touches the lower left corner of the right graph shown in figure 1, i.e., within our numerical precision fcc and bcc are degenerate at the point where $V_\mathrm{R} = 10W$ and $\sigma_\mathrm{R} = 0.2\sigma_\mathrm{Q}$ — the bcc shear modulus is not positive in that domain so that bcc is mechanically unstable. Moreover, σ_Q significantly exceeds a_0 whenever $E_\mathrm{c}(\mathrm{bcc}) > E_\mathrm{c}(\mathrm{fcc})$, which is not physically meaningful. This is why we abstain from identifying stable phases in the domain, where bcc is energetically favorable over fcc.

Despite this negative result, which apparently supports Cleri and Rosato's conclusion [14] that the Gupta potential cannot describe bcc metals, it is somewhat redeeming to notice that parameters pertaining to bcc metals lie in a range where the fcc binding energy merely exceeds that of bcc by $\approx 0.5\%$ or less.

We conclude this section by analyzing in more detail the effect of the cutoff shell as well as that of continuum corrections. The latter is obtained as follows: We assume the same atomic number densities N/V within and outside the radius R_c, at which we cross over from a discrete to a mean-density description. R_c is chosen such that the number density of explicitly included shells within R_c is equal to that outside, i.e., $4\pi R_\mathrm{c}^3/3 = (V/N)(1 + Z_0 + Z_1 + \cdots)$. Instead of summing up individual shell contributions (to either repulsive potential or embedding density), we integrate analytically the respective contribution from R_c to ∞. As a result we obtain effective coordination numbers for repulsion and adhesion, which are second-order polynomial functions of $R_\mathrm{c}/\sigma_\mathrm{R}$ and $R_\mathrm{c}/\sigma_\mathrm{Q}$. Figure 2 confirms that the next-nearest neighbor approximation for $E_\mathrm{c}(\mathrm{fcc})/E_\mathrm{c}(\mathrm{bcc})$ still gives relatively inaccurate fcc-bcc energy differences even with continuum corrections. However, including them gives highly accurate results when truncating after the third shell.

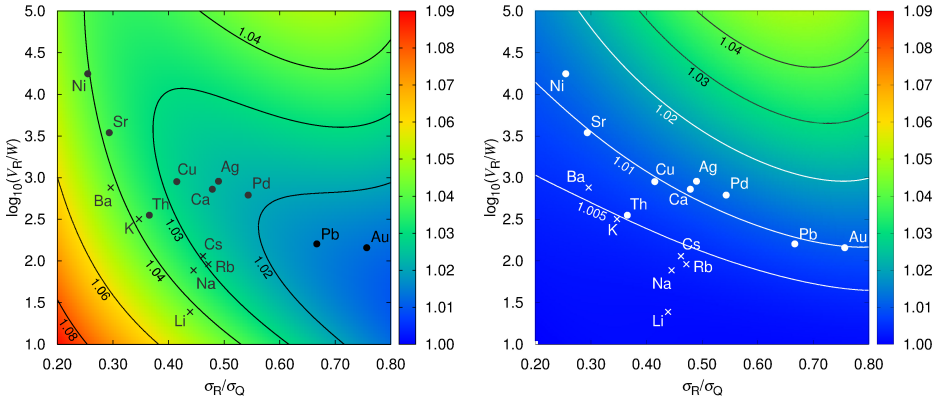

Figure 1. Ratio of the fcc and bcc cohesive energies, $E_c(\text{fcc})/E_c(\text{bcc})$, in the Gupta potential as a function of its two dimensionless numbers σ_R/σ_Q and W/V_R. Left: Next nearest-neighbor approximation without continuum corrections. Right: Direct summation over the eight nearest shells plus a continuum correction. Chemical symbols are placed according to the parameterization of Karolewski [25]. Circles indicate fcc metals while crosses refer to bcc metals.

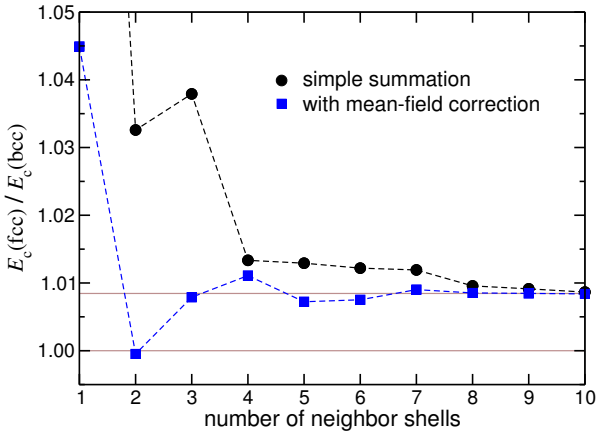

Figure 2. Ratio of fcc and bcc cohesive energies, $E_c(\text{fcc})/E_c(\text{bcc})$, as a function of the number of neighbor shells. Summations are done directly without corrections (black circles) and with continuum corrections (blue squares). Dotted lines are drawn to guide the eye. Solid lines indicate one and the asymptotic energy ratio. The employed parameters reflect copper [11].

3.2. Sutton-Chen embedding density

As for the Gupta-potential, one can simplify the expression for the energy of a crystal when using the potential energy in equation (4). However, this time, there is no closed-form expression for $E_c(\sigma_Q/\sigma_R)$ in the nearest-neighbor approximation. It is yet relatively easy to investigate how σ_Q/σ_R affects $E_c(\text{fcc})/E_c(\text{bcc})$, since our variant of a Sutton-Chen potential depends merely on one dimensionless parameter. To do so, we restrict ourselves to the domain $0 < \sigma_Q/\sigma_R < \{(4/e)^4/6\}^{1/3} \approx 0.92$, in which

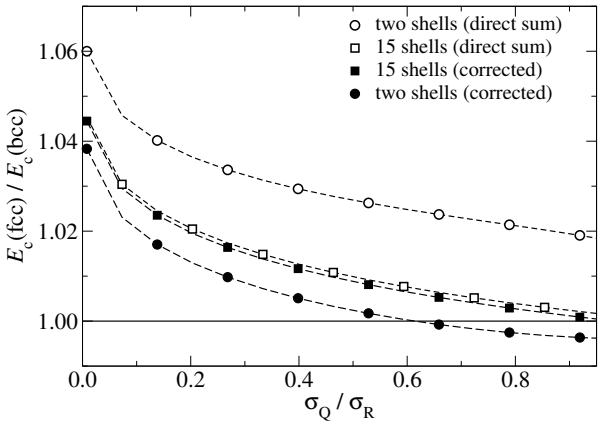

Figure 3. Ratio of fcc and bcc cohesive energies, $E_c(\text{fcc})/E_c(\text{bcc})$, in our variant of a Sutton-Chen potential as a function of the dimensionless number σ_Q/σ_R. Four curves are presented: two shells without corrections (open circles), 15 shells without corrections (open squares), 15 shells with continuum corrections (filled squares) and two shells with continuum corrections (filled circles). The domain is restricted to those values of σ_Q/σ_R in which the dimer has a (relative) energy minimum at finite bond lengths.

a (relative) minimum of the dimer energy occurs at a finite bond length. Throughout this domain, fcc is energetically preferred over both bcc and dimer. The ratio of $a_0(\text{fcc})/\sigma_R$ ranges from roughly eight to thirteen, which lies within the range of values of $a_0(\text{fcc})/\sigma_R$ that Karolewski identified for the Gupta potential.

A central reason for why we investigated Sutton-Chen atomic densities is that they decay less quickly than the exponentials assumed in the Gupta potential. We considered it plausible that this might help to increase the (relative) importance of the second-shell contribution in bcc thereby making bcc stable without having to introduce cutoff functions that usually induce artifacts. Apparently, more care has to be taken in the construction of the embedding density to make this happen. However, we suspect a success in this endeavor to result in quite artificial atomic charge densities, for example, with a shoulder near bcc next-nearest neighbor distances. We therefore expect that reasonably simple and transferable functions cannot favor bcc over fcc in an EAM-type potential and that angular dependencies need to be included, be it implicitly, as in the systematically modified EAM potential [11] or explicitly as in analytical bond-order potentials for bcc materials [29].

4. Vacancy and surface energies

In this section, we analyze what parameters determine the energetic costs for vacancies and surfaces. Since both break perfect periodicity, both shall be labeled as defects hereafter. To rationalize trends, we derive approximate expressions for defect energies in the nearest-shell approximation. They are obtained by assuming that the relaxation of the lattice is only displacive and not reconstructive after the defect has been introduced. Moreover, each atom adjacent to a defect is assigned the optimum cohesive energy for its given coordination number so that we obtain a lower bound for the defect energy in the nearest-neighbor approximation. The analytical treatment

is complemented with numerical results for defects in the next-nearest neighbor approximation by neglecting the lattice relaxation all together. The resulting values constitute upper bounds for defect energies in the next-nearest-shell approximation.

We begin with the analysis of the lower bound for a vacancy energy. Irrespective of the QAT-based potential used, Z_0 (remaining) atoms can no longer be assigned the original binding energy and instead have one neighbor less. Thus,

$$E_\mathrm{v} \lesssim Z_0 E_\mathrm{c}(Z_0) - Z_0 E_\mathrm{c}(Z_0 - 1), \tag{14}$$

i.e., in the nearest-neighbor approximation of the Gupta potential

$$E_\mathrm{v} \lesssim Z_0 \left\{ Z_0^\mu - (Z_0 - 1)^\mu \right\} E_\mathrm{d} \tag{15}$$

$$\approx \mu Z_0^\mu E_\mathrm{d} \quad \text{for large } Z_0. \tag{16}$$

For a short-range two-body potential, a similar estimate for the vacancy energy would have turned out $Z_0 E_\mathrm{d}$ assuming that E_d corresponds again to the cohesive energy per atom in the dimer.

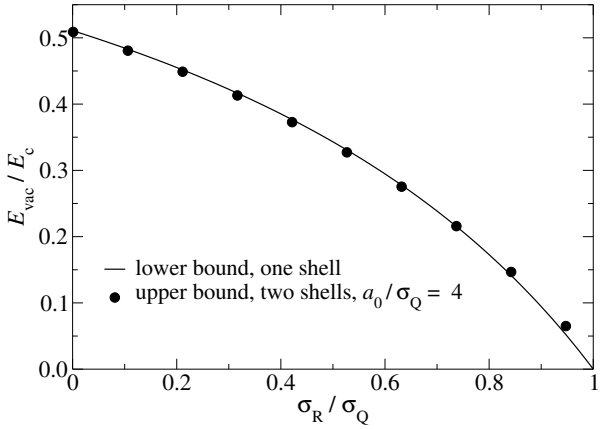

Figure 4. Ratio of the fcc vacancy and fcc cohesive energy per atom, $E_\mathrm{v}/E_\mathrm{c}$, in the Gupta potential as a function of $\sigma_\mathrm{R}/\sigma_\mathrm{Q}$. Lines represent analytical results for the upper bound in the nearest-shell approximation. Symbols refer to numerical results on a lower bound in the next-nearest shell for $a_0 = 4\sigma_\mathrm{Q}$.

Analytical and numerical results for the different bounds on E_v are presented in figure 4. Since our two approaches give quite similar values, we assume that it is legitimate to draw the following conclusion: The ratio of vacancy energy and cohesive energy is predetermined in the Gupta potential once we know the ratio of the dimer energy (or better some other low-coordinated structure such as the linear chain) and the fcc cohesive energy. This conclusion trivially holds for our version of the Sutton-Chen potential, since it only has one dimensionless parameter. However, it should also hold reasonably well for other QAT-based potentials (without square-gradient and related corrections) that approximate not only the elastic tensor of dense structures but also how the cohesive energy as a function of the coordination number down to low-coordinated structures. An interested reader may refer to figure 5 in reference [11] or to figure 1 in reference [17].

Surface energies can be calculated in a similar fashion as vacancy energies. A surface atom missing ΔZ neighbors increases its potential energy by

$$\Delta E_\mathrm{s} \lesssim E_\mathrm{c}(Z_0) - E_\mathrm{c}(Z_0 - \Delta Z), \tag{17}$$

which in the nearest-neighbor Gupta potential becomes

$$\Delta E_{\rm s} \lesssim \{Z_0^{\mu} - (Z_0 - \Delta Z)^{\mu}\}\, E_{\rm d} \tag{18}$$

$$\approx \mu \frac{\Delta Z}{Z_0^{1-\mu}} E_{\rm d} \quad \text{for small } \Delta Z/Z_0. \tag{19}$$

Thus, the lower bound of the surface energy, at this level of approximation, is merely a function of the dimer energy, the ideal bulk coordination number Z_0, and the dimensionless coefficient μ, which itself depends only on $\sigma_{\rm Q}/\sigma_{\rm R}$.

To translate our results into surface energies of the fcc lattice, we need to normalize $\Delta E_{\rm s}(\Delta Z)$ with the area ΔA_{ijk} per surface atom, which depend on the Miller indices (ijk) of the surfaces. Since $(\Delta Z,\, \Delta A/a_0^2)$ is equal to $(3, \sqrt{3}/2)$ for (111), $(6, \sqrt{2})$ for (110), and $(4, 1)$ for (100) surface orientations, one obtains the following surface energies for fcc lattices

$$\gamma_{111}/\tilde{\gamma} = 2\sqrt{3} \tag{20}$$

$$\gamma_{110}/\tilde{\gamma} = 3\sqrt{2} \tag{21}$$

$$\gamma_{100}/\tilde{\gamma} = 4 \tag{22}$$

$$\tag{23}$$

with

$$\tilde{\gamma} \approx \frac{\mu E_{\rm d}}{Z_0^{1-\mu} a_0^2}. \tag{24}$$

keeping the same approximation as in equation (18). More accurate estimates can be obtained by using the correct expression for $\Delta E_{\rm s}$, i.e., equation (17), instead of equation (18) in the calculation of the various surface energies. Representative results are shown in figure 5 for the (111) surface. They are compared again to upper bound estimates in the next-nearest shell approximation. This time the two estimates for the defect energies — normalized to the (surface) atom and expressed in units of the binding energy — are not quite as close as for the vacancy energies. However, in the relevant range of $0.25 < \sigma_{\rm R}/\sigma_{\rm Q} < 0.75$, the agreement is still within 15%. Similar statements can be made about the other surface energies that we investigated for this study, i.e., (100) and (110).

5. Elastic properties of EAM-type potentials

Often, parameters for EAM-type potentials are fitted to the elastic tensor of a given metal. The common believe may be that one can deduce three independent parameters for cubic systems. Here, we show that this is not possible, since one cannot fully adjust three independent tensor elements simultaneously in EAM-type potentials.

5.1. General relations

In this section we reiterate [8, 18, 30, 31] but also extend and simplify analytical expressions for the elastic constants of an EAM crystal with inversion symmetry in which all atoms are equivalent, i.e., we consider a homogeneous deformation characterized by the Eulerian strain tensor ε. The latter relates the coordinate $\mathbf{r}$ of a given material point in the deformed structure to that in the undeformed structure $\mathbf{r}_0$ via

$$\mathbf{r} = (I + \varepsilon)\, \mathbf{r}_0, \tag{25}$$

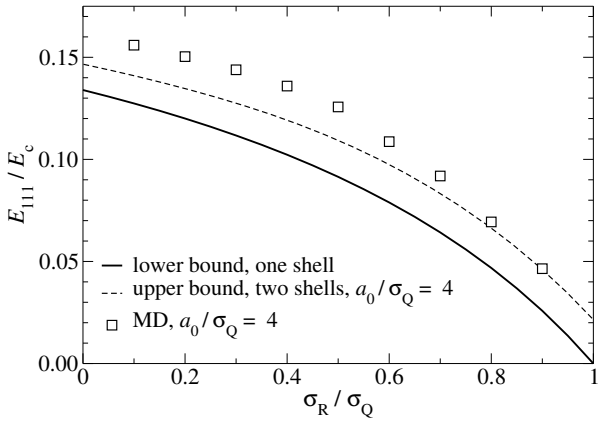

Figure 5. Dimensionless energy per surface atom E_{111}/E_c as a function of σ_R/σ_Q for an fcc Gupta metal. Solid lines refer to numerical results on an upper bound in the next-nearest shell approximation for $a_0/\sigma_R = 4$. Symbols represent numerical data from MD for relaxed structures, also for $a_0/\sigma_R = 4$, and a cutoff including the nearest four shells. Dashed lines represent analytical results for the upper bound in the nearest-shell approximation.

where I is the identity matrix.

The elastic tensor elements can be defined at zero stress, $\partial U_T/\partial\epsilon_{\alpha\beta} = 0$, as

$$C_{\alpha\beta\gamma\delta} = \frac{1}{V}\,\frac{\partial^2 U_T}{\partial\epsilon_{\alpha\beta}\partial\epsilon_{\gamma\delta}}, \tag{26}$$

where V is the total volume of the N-particle system. After some algebra, one obtains for periodically repeated systems in mechanical equilibrium [8],

$$\begin{aligned}\frac{V}{N}C_{\alpha\beta\gamma\delta} = &\sum_j \left\{r_{ij}^2 U_R''(r_{ij}) - r_{ij}U_R'(r_{ij})\right\} n_{ij,\alpha\beta\gamma\delta} \\ &+ F'(\rho_i)\sum_j \left\{r_{ij}^2\phi''(r_{ij}) - r_{ij}\phi'(r_{ij})\right\} n_{ij,\alpha\beta\gamma\delta} \\ &+ F''(\rho_i)\sum_{j,k} r_{ij}r_{ik}\phi'(r_{ij})\phi'(r_{ik}) n_{ij,\alpha\beta}n_{ik,\gamma\delta}\end{aligned} \tag{27}$$

with

$$n_{ij,\alpha\beta\ldots} \equiv \frac{r_{ij,\alpha}}{r_{ij}}\,\frac{r_{ij,\beta}}{r_{ij}}\ldots \tag{28}$$

To proceed further, it is beneficial to regroup the sums on the r.h.s. of equation (27) as sums over individual shells. One then needs to evaluate each function only once at a given shell distance, e.g., at a_0 for the nearest-neighbor shell ($s = 0$), or at a_1 for the next shell ($s = 1$), etc. This way, the effect of shell geometry and occupancy is expressed by the term $n^{(s)}_{\alpha\beta\ldots}$ defined in equation (33). Specifically,

$$\begin{aligned}\frac{V}{N}C_{\alpha\beta\gamma\delta} = &\sum_s \left\{f(a_s) + F'(\rho_i)g(a_s)\right\} n^{(s)}_{\alpha\beta\gamma\delta} \\ &+ F''(\rho_i)\sum_s h(a_s)n^{(s)}_{\alpha\beta}\sum_s h(a_s)n^{(s)}_{\gamma\delta}\end{aligned} \tag{29}$$

with

$$f(a_s) = a_s^2 U_{\mathrm{R}}''(a_s) - a_s U_{\mathrm{R}}'(a_s) \tag{30}$$

$$g(a_s) = a_s^2 \phi''(a_s) - a_s \phi'(a_s) \tag{31}$$

$$h(a_s) = a_s \phi'(a_s) \tag{32}$$

$$n^{(s)}_{\alpha\beta\ldots} = \sum_{j\in s} \frac{r_{ij,\alpha}}{r_{ij}} \frac{r_{ij,\beta}}{r_{ij}} \ldots \tag{33}$$

From equation (29), it becomes immediately clear — as originally discussed by Daw and Baskes [8] — that the elastic tensor is fully symmetric in all four indices when $F''(\rho)$ disappears, in which case the embedding function is linear and interactions subsequently pairwise. In other words, the Cauchy relations would hold, e.g., $C_{1212} = C_{1122}$, or, in Voigt notation, $C_{44} = C_{12}$ for cubic systems. However, embedding functions usually have a positive curvature so that $C_{1122} > C_{1212}$. This inequality is certainly not universally valid; including strain-induced charge transfer between ions usually induces the opposite sign, i.e., $C_{1122} < C_{1212}$ [32].

Table 1 lists the numerical values of the non-vanishing tensor elements $n^{(0)}_{\alpha\beta}$ and $n^{(0)}_{\alpha\beta\gamma\delta}$ for fcc, bcc, and sc. It enables one, together with equation (29), to evaluate the elastic tensor for a cubic structure described by EAM-type potentials without much bookkeeping up to the next-nearest-neighbor approximation. This is because the next-nearest shell of fcc, bcc, and sc have the nearest-neighbor shell topology of sc, again sc, and fcc, respectively. For bcc and sc one could even go one shell further, since their $s = 2$ shell topography is fcc and bcc-like, respectively. To include the $s = 2$ fcc shell, table 1 would have to be extended with a sum over directors proportional to $(\pm 2, \pm 1, \pm 1)$.

	$n^{(0)}_{11}$	$n^{(0)}_{1111}$	$n^{(0)}_{1122}$
fcc	4	2	1
bcc	8/3	8/9	8/9
sc	2	2	0

Table 1. Non-zero nearest shell tensor elements $n^{(0)}_{\alpha\beta\ldots}$. $n^{(0)}_{22}$, $n^{(0)}_{2222}$, etc. are obtained by symmetry. The symmetry of the next-nearest shell is sc for fcc and bcc so that $n^{(1)}_{11}(\mathrm{fcc}) = n^{(1)}_{11}(\mathrm{bcc}) = n^{(0)}_{11}(\mathrm{sc})$.

Although Cauchy relations do not hold for EAM-type potentials, cubic systems only have two independent elastic constants in the (dominant) nearest-neighbor approximation. From equation (29) and table 1 one can deduce in a straightforward manner that the so-called tetragonal shear modulus defined as

$$C_{\mathrm{S}} = \frac{C_{11} - C_{12}}{2} \tag{34}$$

is subject to the following constraints

$$C^{(0)}_{\mathrm{S}}(\mathrm{fcc}) = \frac{C^{(0)}_{44}(\mathrm{fcc})}{2} \tag{35}$$

$$C^{(0)}_{\mathrm{S}}(\mathrm{bcc}) = 0. \tag{36}$$

Since isotropic materials automatically satisfy $C_{\mathrm{S}} = C_{44}$, the (relative) deviation of C_{S} from C_{44} can be seen as a measure of elastic anisotropy.

Including more distant shells formally lifts this limitation of EAM-type potentials. Since both fcc and bcc have a next-nearest neighbor shell topology identical to the nearest-neighbor simple-cubic shell, the following leading-order correction applies in either case

$$\frac{V}{N}\Delta C_{\mathrm{S}}^{(1)} = f(a_1) + F'(\rho_i)g(a_1) \tag{37}$$

with which the shear modulus in the $s = 1$ approximation becomes $C_{\mathrm{S}}^{(1)} = C_{\mathrm{S}}^{(0)} + \Delta C_{\mathrm{S}}^{(1)}$. It is not *a-priori* possible to predict how large the $\Delta C_{\mathrm{S}}^{(1)}$ corrections are in practice. However, at least for fcc, they should be small for similar reasons as why next-nearest neighbors do not contribute much to the cohesive energy. The relative importance of the corrections in bcc might be slightly larger. To investigate the issue further, we analyze the elastic tensor in more detail in the context of the Gupta potential and our variant of the Sutton-Chen potential.

5.2. Gupta potential

The specific functional form of the Gupta potential induce constraints for the (nearest-neighbor) elastic constants in addition to those mentioned in equations (35) and (36). They can be derived in closed form if we use a_0 at equilibrium rather than W as natural variable. The elastic tensor in the nearest-shell approximation then simply reads

$$C_{\alpha\beta\gamma\delta}^{(0)} = \tilde{C}\left\{\left(1 - \frac{\sigma_{\mathrm{R}}}{\sigma_{\mathrm{Q}}}\right) n_{\alpha\beta\gamma\delta}^{(0)} + \frac{1}{2Z_0}\frac{\sigma_{\mathrm{R}}}{\sigma_{\mathrm{Q}}} n_{\alpha\beta}^{(0)} n_{\gamma\delta}^{(0)}\right\} \tag{38}$$

with

$$\tilde{C} = \frac{N}{V}\frac{a_0^2}{\sigma_{\mathrm{R}}^2}\frac{\tilde{V}_{\mathrm{R}}}{2}. \tag{39}$$

Thus, ratios of the elastic tensor elements in the nearest-shell approximation of a given crystalline structure are fully determined by $\sigma_{\mathrm{Q}}/\sigma_{\mathrm{R}}$, just like the ratios of the various defect energies. For example, the orientationally averaged shear modulus $G \equiv (C_{\mathrm{S}} + C_{44})/2$ can be written as

$$G^{(0)}(\mathrm{fcc}) = \frac{9}{8}\mu B^{(0)}(\mathrm{fcc}) \tag{40}$$

$$G^{(0)}(\mathrm{bcc}) = \mu B^{(0)}(\mathrm{bcc}). \tag{41}$$

Analytical expressions for $C_{\alpha\beta\gamma\delta}^{(1)}$ are more involved than for the elastic tensor in the nearest-neighbor shell approximation (an interested reader is referred to the electronic supplement). We abstain from giving them here and instead show results graphically in figure 6. Since results for dimensionless quantities may now also depend on W/V_{R}, we need to assign reasonable ratios for that quotient. This is done by constraining $a_0(\mathrm{fcc})/\sigma_{\mathrm{Q}}$ to representative values for reasons stated in section 2. As discussed in more detail in the conclusions section, the precise value of a_0/σ_{Q} does not affect many dimensionless properties in a significant fashion, except perhaps when numbers are "small" such as the relative difference between fcc and bcc cohesive energies.

Although the ratio G/B appears rather insensitive to the specific value of μ, the relative contribution of C_{44} and C_{S} to their average G can be affected in a non-negligible way by next-nearest neighbors. This is because the contribution of the

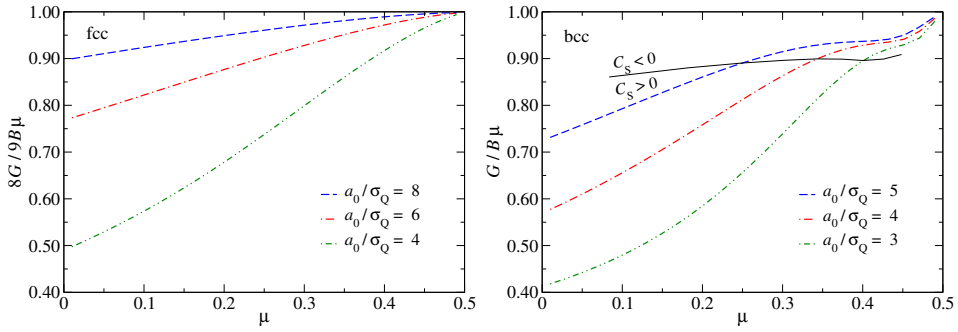

Figure 6. Dimensionless ratios $8G/9B\mu$ (fcc, left figure) and $G/B\mu$ (bcc, right figure) as a function of the coefficient μ for representative values of a_0/σ_Q. In the nearest-neighbor approximation, both ratios equal one. Maximum and minimum values for a_0/σ_Q were chosen to represent roughly the extreme values identified by Karolewski. For bcc the full black line indicates the values of μ, where the tetragonal shear modulus changes sign.

next-nearest shell (which is simple cubic for both fcc and bcc) is small (actually zero) for C_{44} but relatively large for C_S. This is opposite to the trend of the nearest-neighbor shells in fcc and bcc. Pertinent results are presented in section 6.

6. Comparison of dimensionless materials properties

In this section, we analyze how well different metals obey the correlations that we found to be intrinsic to the Gupta potential. Towards this end, we express by default elastic tensor elements in units of the bulk modulus, and all energies, including thermal energies, e.g., $k_B T_m$, in units of the cohesive energy. Quantities normalized in this way will be called reduced quantities, e.g., the reduced shear modulus for a bcc metal would read $\tilde{C}_{44} \equiv C_{44}(\text{bcc})/B(\text{bcc})$.

We first analyze to what degree it is possible to correlate the regular, reduced shear modulus $\tilde{C}_{44}$ with the symmetrized, reduced shear modulus $\tilde{G}$. Mechanical stability not only demands both to be positive but also $\tilde{C}_{44}$ to be less than $\tilde{G}/2$ since otherwise the tetragonal shear modulus would not be positive. Fig. 7 reveals that the linear relation — as obtained for the Gupta potential in the nearest-shell approximation — is a reasonable approximation to the full Gupta potential without truncation. Also many experimental results appear to be consistent with the conveyed trend for the fcc structure. If we allow for a relative deviation of 10% for individual elastic constants, then all elements would be in a range covered by the Gupta potential. Only a few of the considered fcc metals (Th, Rh, Ir, Sr) are outside the range that is feasible within a Gupta description. The corresponding values still obey the nearest-neighbor prediction $G = 3C_{44}/4$ reasonably well.

In contrast to fcc, bcc structures are described relatively poorly and deviations of experimental data from the theoretical curve are substantial. While some elements (Li, Na, K, Rb, Cs) appear close to the allowed C_{44}/B values, they all assume values for G/B for which Gupta bcc is mechanically unstable. This further substantiates the old finding by Cleri and Rosato [14] that Gupta is not appropriate for bcc metals. One may yet notice that the trend appears correct, i.e., a small shift of the Gupta lines by $\Delta G/B = 0.2$ to the right would nicely reflect the experimentally observed trends and

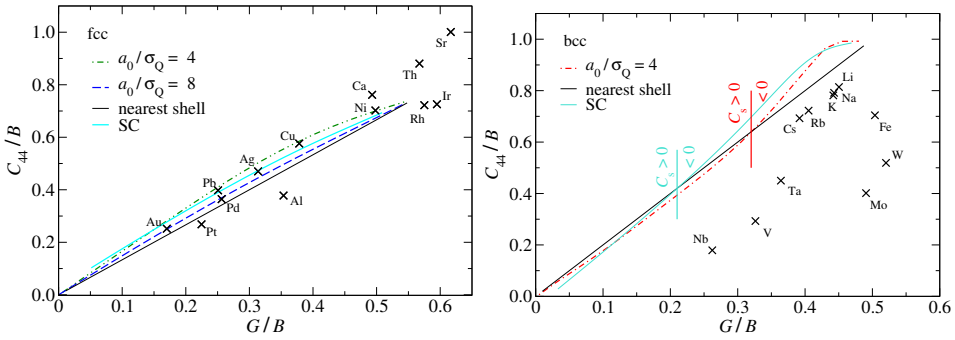

Figure 7. Reduced shear modulus C_{44}/B as a function of the reduced symmetrized shear modulus G/B for fcc (left) and bcc (right). For bcc, vertical lines indicate the change of sign for C_S. Experimental results are included for selected elements (Ag [33], Al [33], Au [33], Ca [34], Cs [33], Cu [33], Fe [33], Ir [33], K [33], Li [33], Mo [33], Na [33], Ni [33], Nb [33], Pb [33], Pd [33], Pt [33], Rb [33], Rh [35], Sr [36], Ta [33], Th [33], V [33], W [33]). Values for Ba {bcc, (0.878,0.781) [36]} and Cr {bcc, (0.668,0.406) [33]} lie outside the presented region. Experimental data was selected for the lowest available temperature.

only few of the bcc elements (Mo, W, Ba, Cr) would remain far from the curve.

To better unravel relative errors of the shear modulus, we normalize C_{44} with the symmetrized shear modulus C_S times a constant factor, which is chosen such that the ratio yields one in the nearest-neighbor approximation, see figure 7. For fcc, the nearest-neighbor predictions remain within 20% accuracy in the relevant range of $G/B > 0.2$. Corrections to the nearest-neighbor approximation in bcc are even smaller. However, the discrepancy between the theoretical and experimental values of C_{44}/G in bcc metals becomes particularly apparent in this representation. It also becomes clear that changing the functional form of the atomic densities from exponential in the Gupta to $1/R^6$ does not allow one to alter trends, at least not in the practically relevant domain of $G/B > 0.2$.

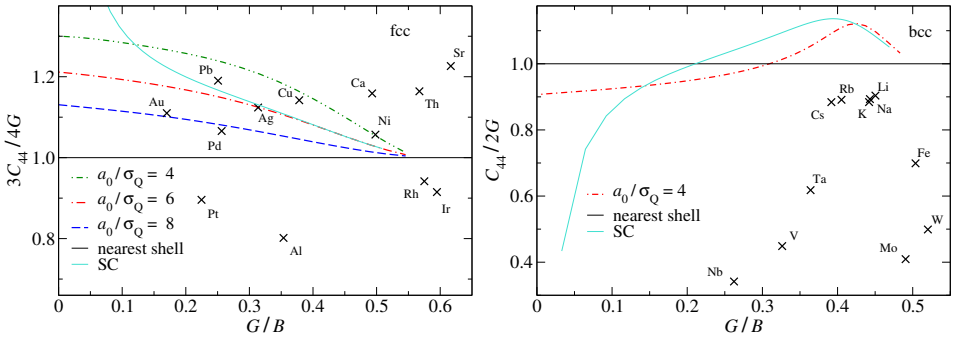

Figure 8. Measure for the relative contribution of C_{44} to the orientationally averaged shear modulus $G \equiv (C_{44} + C_S)/2$ as a function of G/B for fcc (left) and bcc (right). The measure is normalized such that the nearest-neighbor shell approximation is equal to one. Systems with bcc structure are mechanically unstable when $C_{44}/2G$ exceeds one. Values for Ba {bcc, (0.878,0.781) [36]} and Cr {bcc, (0.668,0.406) [33]} lie outside the presented region.

We proceed with the analysis of vacancy energies in figure 9. Unfortunately, experimental data appears to be plagued with large uncertainties. Estimates for E_v deviate by as much as a factor of two between different methods. For example, positron measurements report the values of 3.0 eV for Mo [37], while the specific heat ones – 2.24 eV [38] (with 1.6 eV when extrapolated to zero temperatures). Some interesting observations can yet be made. Results for fcc metals appear to be in the correct ball park for a fair fraction of the considered fcc metals. Even the Gupta results most inconsistent with experiments are still much more accurate than those that one would obtain with two-body potentials. In the latter case, E_v automatically turns out smaller than but close to E_c, e.g., in the fcc nearest-neighbor approximation $11E_\mathrm{c}/12 \leq E_\mathrm{v} \leq E_\mathrm{c}$. More interesting may be that the results for most considered bcc metals would have again been quite satisfactory if the theoretical results could be shifted to slightly larger values of $\Delta G/B$.

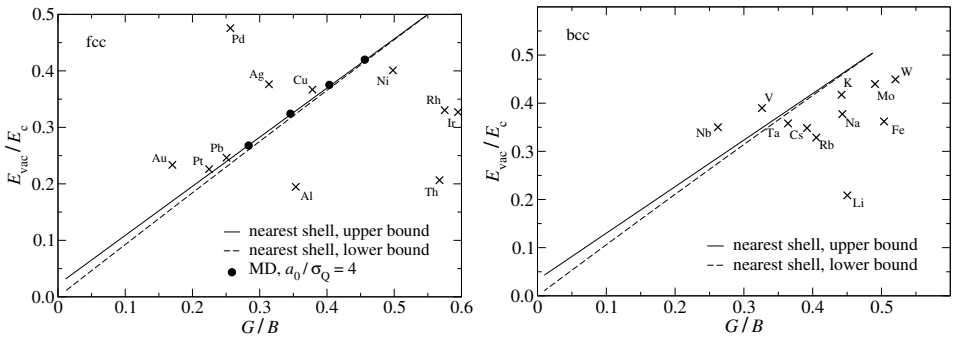

Figure 9. Dimensionless vacancy energy $E_\mathrm{v}/E_\mathrm{c}$ as a function of G/B for fcc (left) and bcc (right). Full lines show the lower-bound estimates in the nearest-neighbor approximation. Filled squares represent results from molecular dynamics simulations. Experimental results are included for selected elements (cohesive energies are taken from Kittel's book [39]; vacancy energies are provided for: Ag [37], Al [37], Au [37], Cs [40], Cu [37], Fe [37], Ir [41], K [40], Li [40], Mo [37], Na [40], Nb [37], Ni [37], Pb [37], Pd [37], Pt [37], Rb [42], Rh [41], Ta [37], Th [43], V [37], W [37]). Values for Cr {bcc, (0.668,0.488) [37]} lie outside the presented region.

We next investigate surface energies for fcc metals in figure 10, where we excluded data on bcc — as well as in a later analysis of melting temperatures — because bcc Gupta is mechanically unstable, or at best marginally stable, for most G/B values of interest. Trends on surface energies, or more precisely, on energy per (111) surface atom, are consistent with those on vacancy energies. Whenever E_{111}/E_c is (much) above or below the predicted value at that ratio of G/B, so is $E_\mathrm{v}/E_\mathrm{c}$. Yet, the only fcc metal, for which defect energies are off by a factor of two, is palladium.

Up to this point, we have focused on dimensionless quantities that depend only on G/B in the nearest-shell approximation of the Gupta potential. For these quantities, one would therefore expect little sensitivity on W/V_R, or, alternatively on a_0/σ_Q. One quantity that however does depend on a_0/σ_Q is the cohesive energy density expressed in units of the bulk modulus, i.e., E_c/BV_0. In the nearest-shell approximation, one obtains for bcc and fcc — just as for simple cubic, diamond, and hcp — that

$$\frac{E_\mathrm{c}}{BV_0} = 18\frac{\sigma_\mathrm{Q}\sigma_\mathrm{R}}{a_0^2} \tag{42}$$

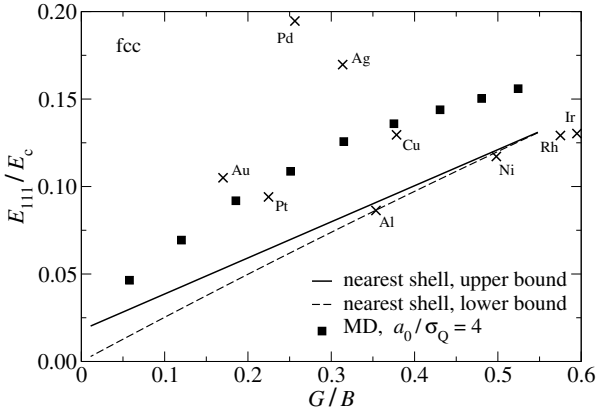

Figure 10. Dimensionless energy per surface atom E_{111}/E_c as a function of G/B. Solid line corresponds to the lower bound in the nearest-neighbor approximation. Bold squares represent numerically exact data for relaxed structures, also for $a_0/\sigma_R = 4$, and a cutoff including the nearest four shells. Experimental values for the surface energies are taken from Ref. [44].

Numerical and experimental results for E_c/BV_0 are presented as a function of G/B in figure 11. For fcc metals, one can see that most elements – at least those with $G/B < 0.5$, i.e., those potentially consistent with Gupta – are consistent with values of a_0/σ_Q between four and eight, which is the range of values that Karolewski found to be useful as well. Regarding bcc metals, one can observe that experimental data for most considered elements would again only lie within the "allowed domain" if we could shift the theoretical curves to slightly larger values of G/B.

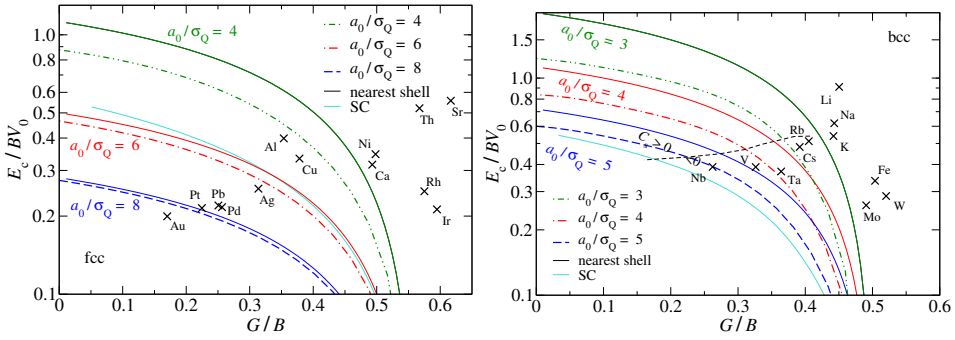

Figure 11. Dimensionless cohesive energy E_c/BV_0 as a function of G/B for fcc (left) and bcc (right). Full lines refer to the nearest-shell approximation. The tetragonal shear modulus, C_S, is negative in the bcc phase for G/B values to the left from the black dashed line for Gupta potential. For the Sutton-Chen variant of the potential the critical value is $G/B \approx 0.21$. Ba [bcc, (0.878, 0.557)] and Cr [bcc, (0.668,0.281)] are outside of the presented region and are excluded from the graph.

The last dimensionless quantity that we analyze in this paper is the reduced thermal energy at the melting temperature, $k_B T_m/E_c$, as a function of G/B in figure 12. Some elements behave in agreement with the trends revealed in figure 11,

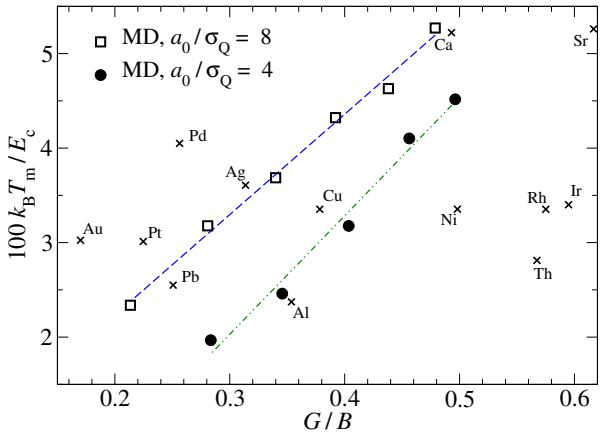

Figure 12. Thermal energy at the melting point $k_B T_m$ (times hundred) in units of cohesive energy per atom as a function of the dimensionless symmetrized shear modulus G/B. Open squares correspond to the value of $a_0/\sigma_Q = 8$, filled circles – to the value of $a_0/\sigma_Q = 4$. Lines are drawn to guide the eye. Experimental results are included for selected elements (melting temperatures are taken from Kittel's text book [39])

e.g., Au, Pt, Pb, and Pd all lie close to the $a_0/\sigma_Q = 8$ line. However, other elements, in particular Ca, would get assigned different values for σ_Q/a_0 from figures 11 and 12, which implies that calcium, amongst other metals, cannot be described to large accuracy with Gupta or related potentials.

It is interesting to observe that there is an essentially linear trend of $k_B T/E_c$ with G/B within the Gupta potential for a fixed value of a_0/σ_Q. It might be possible to rationalize this as follows: Defects become numerous in the crystal before they melt and are frequently seen as nuclei for the transition to occur. The energy of isolated defects, in particular that of dislocations, tends to have one contribution from the core and another one from the elastic deformation outside the core. While (dimensionless) core and elastic contributions supposedly depend linearly on μ – at least in the nearest-shell contribution – their relative weight should depend on a_0/σ_Q, since this ratio affects E_c/BV_0. Once this relative weight is fixed, both defect and elastic energy scale linearly with μ.

7. Discussion and Conclusions

In this work, we have analyzed the origin of the correlation between various (dimensionless) materials properties predicted by the Gupta potential for monoatomic systems. We chose the Gupta potential for mainly two reasons: In the class of EAM-like potentials, it has best described elemental systems with largely varying coordination number. More importantly, many properties can be expressed analytically within the nearest-neighbor approximation in terms of the four parameters that fully determine the potential for an individual element. This allows one to cover the possible parameter space quite easily. Since two parameters of a potential energy surface can be used to define the units for energy and length, two dimensionless parameters remain, which then fully determine the dimensionless properties of the element under consideration. Here, we find that only one of the two dimensionless

parameters is truly significant for many dimensionless properties, namely the ratio $\sigma_{\rm R}/\sigma_{\rm Q}$, or, alternatively the coefficient $\mu = (1-\sigma_{\rm R}/\sigma_{\rm Q})/(2-\sigma_{\rm R}/\sigma_{\rm Q})$. For a given value of μ, many dimensionless properties, such as G/B, $E_{\rm c}(Z)/E_{\rm c}(Z=1)$, $E_{\rm v}/E_{\rm c}$, or surface energies (in units of $E_{\rm c}/a_0^2$) are predetermined within a few percent and relatively insensitive to the ratio $V_{\rm R}/W$.

At first sight, it might be surprising that the ratio $V_{\rm R}/W$ does not allow one to fine tune many (dimensionless) materials properties in a significant fashion. We rationalize this as follows: rather than taking $V_{\rm R}/W$ as the second dimensionless parameter of the Gupta potential, one may as well use the ratio $a_0/\sigma_{\rm Q}$. This latter number essentially only affects to what extent next-nearest or more distant neighbors contribute to the embedding density, or, in an even lesser way, to the repulsive potential. In chemically relevant parameterization, $a_0/\sigma_{\rm Q} \gtrsim 4$ so that the relative contribution of nearest neighbors to the total embedding density is $\gtrsim 80\%$. Thus, the second dimensionless parameter cannot be used to fine tune meaningfully all those properties that only depend on the coefficient μ in the nearest-neighbor approximation. In fact, any reasonable parameterization should reflect that the *direct* effect of next-nearest or further neighbors on a central (fcc) embedding site must be small. In sophisticated bond-order potentials [45], which like EAM-type potentials contain a second-moment, tight-binding approximation as a limiting case [46], the direct influence of non-nearest atoms on a central atom is actually screened. The one important effect that the ratio $a_0/\sigma_{\rm Q}$ does have is that the ratio $E_{\rm c}/BV_0$ can be tuned with it. This in turns affects, for example, the relative contributions of a dislocation energy coming from its core and the elastic displacement field.

One might wonder to what degree the insights gained for the Gupta potentials pertain to related potentials. While details might differ, we argue that (rough) trends should be similar for the following reason: In any reasonable parameterization, the nearest-neighbor shell dominates all other shells. At typical nearest-neighbor distances, one should then be in a position to approximate the repulsive interactions as well as the charge densities by exponentials. The second-order derivatives might deviate by perhaps as much as 30%, but not by large factors. The one single expression that might allow for more flexibility is the embedding function. We would yet expect that it is possible to approximate $F(\rho)$ with a polynomial $F \propto \rho^d$ around typical embedding densities and that the exponent d is not too different from 1/2. At least, in our experience, allowing d to differ from 1/2 does not lead to substantial improvements. For these reasons all accurate EAM-type potentials should reveal similar trends as the Gupta potential. This expectation was met by our variant of a Sutton-Chen potential, which revealed slightly different numbers than Gupta but almost identical trends.

Our claim that findings for the Gupta potential relate to all conventional QAT-based potentials can certainly be challenged: Dai *et al.* [28] developed a rather simple Finnis-Sinclair type potential, which seems to work better for bcc metals than we appear to deem possible. Although we see their potentials as valuable and do not hesitate to recommend their use, we also have two points of fundamental criticism: First, the charge density is expanded into powers of $(r-d)$, for interatomic distances r below the cutoff $d \gtrsim 4$ Å and set to zero outside the interaction range. Thus, the total interaction between two atoms is non-attractive for interatomic distance exceeding d, which is incorrect and supposedly problematic for simulation of systems other than bulk materials. Second, the elastic constants computed for zero temperature are compared to those measured experimentally at finite temperature. Though this is frequently done, it is quite problematic. The shear elastic constants can change

to a non-negligible degree in this temperature range. For example, for potassium, $\tilde{G}_{44}(T = 300\ \mathrm{K}) \approx 0.32$, which is close to the value achieved in the potential of Dai *et al.*, while the true target should be $\tilde{G}_{44}(T = 4\ \mathrm{K}) \approx 0.44$.

How does this work help to identify parameters for a specific element? If various target quantities are known, one can check if the correlation between them correspond to those of the Gupta potential presented here. The supposedly best number to get a first estimate for μ is the ratio G/B. If other dimensionless observables that are also expected to depend only on μ deviate strongly from their expected value, neither the bare Gupta potential nor another conventional EAM-type potential will be a good choice. If, however, the match is reasonable, one may proceed by fixing the second dimensionless coefficient, W/V_R or alternatively, σ_R/a_0. This can be done by adjusting the respective numbers such that the desired value of the reduced bulk modulus, BV_0/E_c, is matched. If only T_m but not E_c is known reliably, which is sometimes the case, one might want to estimate E_c from T_m and μ. Alternatively, one can fit to the equation of state up to high pressures, which also helps in identifying the ratio W/V_R. Once the two dimensionless variables are fixed, it is straightforward to set the absolute value of σ_Q by choosing it such that the potential matches the lattice constant. Next, one can chose the prefactor W to reproduce, for example, the bulk modulus.

A revealing result of our work is that some bcc materials appear to be almost consistent with the Gupta potential except for two issues: Without problematic cutoffs, the predicted fcc energy is always slightly larger than for bcc, while in reality, this ordering is, by definition, the other way around. In addition, the computed values for G/B at zero temperature are very often around 20% smaller than experimental values. To fix the fcc versus bcc energy issue, we only need a small perturbation that reverses the order of fcc and bcc cohesive energies without changing anything much else. One possibility to achieve this is to include corrections to the embedding function that depend on the fourth-order derivatives of the charge density, which is the lowest-order tensor entering a QAT potential expansion allowing one not only to lift the (quasi) degeneracy of fcc and hcp but also to favor bcc and eventually simple cubic over fcc or hcp [11]. Once bcc is more stable than fcc, the tetragonal shear modulus no longer disappears in the nearest-neighbor approximation, which in turn might help to solve the problem that the (zero-temperature) G/B ratio is generally too small for bcc metals. We plan on investigating these expectations in the future.

Acknowledgments

We thank the Jülich Supercomputing Centre for computing time on JUQUEEN and JUROPA.

[1] Kelchner C L, Plimpton S J and Hamilton J C 1998 *Phys. Rev. B* **58** 11085–11088
[2] Mishin Y, Mehl M J, Papaconstantopoulos D A, Voter A F and Kress J D 2001 *Phys. Rev. B* **63** 224106
[3] Hoyt J J, Asta M and Karma A 2003 *Mat. Sci. Eng. R* **41** 121–163
[4] Szlufarska I 2006 *Mater. Today* **9**
[5] Jin Z H, Gumbsch P and Albe K 2008 *Acta Mater.* **56**
[6] Stott M J and Zaremba E 1980 *Phys. Rev. B* **22** 1564
[7] Daw M S and Baskes M I 1983 *Phys. Rev. Lett.* **50** 1285–1288
[8] Daw M S and Baskes M I 1984 *Phys. Rev. B* **29** 6443–6453
[9] Daw M S, Foiles S M and Baskes M I 1993 *Mat. Sci. Rep.* **9** 251–310
[10] Wu G, Lu G, Garcia-Cervera C J and E W 2009 *Phys. Rev. B* **79** 035124
[11] Jalkanen J and Müser M H 2015 *Model. Simul. Mater. Sc. Eng.* **23** 074001

[12] Gupta R P 1981 *Phys. Rev. B* **23** 6265–6270
[13] Tománek D, Mukherjee S and Bennemann K H 1984 *Phys. Rev.* **28** 665–673
[14] Cleri F and Rosato V 1993 *Phys. Rev. B* **48** 22–33
[15] Ercolessi F, Tosatti E and Parrinello M 1986 *Phys. Rev. Lett.* **57** 719
[16] Finnis M W and Sinclair J E 1984 *Phil. Mag. A: Cond. Matt.* **50** 45–55
[17] Robertson I J, Heine V and Payne M C 1993 *Phys. Rev. Lett.* **70** 1944–1947
[18] Paidar V, Larere A and Priester L 1997 *Model. Simul. Mater. Sc. Eng.* **5** 381–390
[19] Methfessel M, Hennig D and Scheffler M 1992 *Phys. Rev. B* **46** 4816–4829
[20] Haftel M I 1993 *Phys. Rev. B* **48** 2611–2622
[21] Rodríguez A M, Bozzolo G and Ferrante J 1993 *Surf. Sci.* **289** 100–126
[22] Pasianot R and Savino E J 1992 *Phys. Rev. B* **45** 12704–12710
[23] Zhou L G and Huang H 2013 *J. Engr. Mater. Tech.* **135** 11010
[24] Sutton A P and Chen J 1990 *Phil. Mag. Lett.* **61** 139–146
[25] Karolewski M A 2001 *Radiat. eff. defect s.* **153** 239–255
[26] Norskov J K and Lang N D 1980 *Phys. Rev. B* **21** 2131–2136
[27] Johnson R A and Oh D J 1989 *J. Mater. Res.* **4** 1195–1201
[28] Dai X D, Kong Y, Li J H and Liu B X 2006 *J. Phys.: Condens. Matter* **18** 4527 – 4542
[29] Müller M, Erhart P and Albe K 2007 *J. Phys.: Condens. Matter* **19** 326220
[30] Johnson R A 1988 *Phys. Rev. B* **37** 3924–3931
[31] Oh D J and Johnson R A 1988 *J. Mater. Res.* **3** 471–478
[32] Sukhomlinov S V and Müser M H 2015 *J. Chem. Phys.* **143** 224101
[33] Simmons G and Wang H 1971 *Single Crystal Elastic Constants and Calculated Aggregated Properties* (Cambridge: MIT Press)
[34] Stassis C, Zaretsky J, Misemer D K, Skriver H L, Harmon B N and Nicklow R M 1983 *Phys. Rev. B* **27** 3303–3307
[35] Walker E, Ashkenazi J and Dacorogna M 1981 *Phys. Rev. B* **24** 2254–2256
[36] Buchenau U, Heiroth M, Schober H R, Evers J and Oehlinger G 1984 *Phys. Rev. B* **30** 3502–3505
[37] Schaefer H E 1987 *Phys. Stat. Sol. (a)* **102** 47 – 65
[38] Kraftmakher Y 1998 *Phys. Rep.* **299** 79 – 188
[39] Kittel C 2005 *Introduction to Solid State Physics, 8th ed.* (New York: Wiley)
[40] Stott M J 1978 *J. Nucl. Mater.* **69-70** 157 – 175
[41] Ouyang Y, Chen H and Zhong X 2003 *J. Mater. Sci. Technol.* **19** 243 – 246
[42] McDonald D K C 1955 *Defects in Crystalline Solids* (London: Phys. Soc.)
[43] Kim S M, Jackman J A, Buyers W J L and Peterson D T 1984 *J. Phys. F: Met. Phys.* **14** 2323 – 2328
[44] de Boer F R, Boom R, Mattens W C M, Miedema A R and Niessen A K 1988 *Cohesion in Metals* (Elsevier)
[45] Pastewka L, Klemenz A, Gumbsch P and Moseler M 2013 *Phys. Rev. B* **87** 205410
[46] Drautz R, Hammerschmidt T, Cak M and Pettifor D G 2015 *Model. Simul. Mater. Sc. Eng.* **23** 074004